entropy

MDPI

Article

Maximum Exergetic Efficiency Operation of a Solar Powered H_2O-LiBr Absorption Cooling System

Camelia Stanciu [1,*], Dorin Stanciu [1], Adina-Teodora Gheorghian [1], Elena-Beatrice Tănase [1], Cătălina Dobre [1] and Marius Spiroiu [2]

1 Department of Engineering Thermodynamics, University Politehnica of Bucharest, Bucharest 060042, Romania; dorin.stanciu@upb.ro (D.S.); adina.gheorghian@upb.ro (A.-T.G.); elena.tanase0604@upb.ro (E.-B.T.); catalina.dobre@upb.ro (C.D.)

2 Department of Rolling Stock, University Politehnica of Bucharest, Bucharest 060042, Romania; marius.spiroiu@upb.ro

* Correspondence: camelia.stanciu@upb.ro; Tel.: +40-21-402-9339

Received: 22 October 2017; Accepted: 6 December 2017; Published: 9 December 2017

Abstract: A solar driven cooling system consisting of a single effect H_2O-LiBr absorbtion cooling module (ACS), a parabolic trough collector (PTC), and a storage tank (ST) module is analyzed during one full day operation. The pressurized water is used to transfer heat from PTC to ST and to feed the ACS desorber. The system is constrained to operate at the maximum ACS exergetic efficiency, under a time dependent cooling load computed on 15 July for a one storey house located near Bucharest, Romania. To set up the solar assembly, two commercial PTCs were selected, namely PT1-IST and PTC 1800 Solitem, and a single unit ST was initially considered. The mathematical model, relying on the energy balance equations, was coded under Engineering Equation Solver (EES) environment. The solar data were obtained from the Meteonorm database. The numerical simulations proved that the system cannot cover the imposed cooling load all day long, due to the large variation of water temperature inside the ST. By splitting the ST into two units, the results revealed that the PT1-IST collector only drives the ACS between 9 am and 4:30 pm, while the PTC 1800 one covers the entire cooling period (9 am–6 pm) for optimum ST capacities of 90 kg/90 kg and 90 kg/140 kg, respectively.

Keywords: solar cooling; fully mixed mass storage; exergetic efficiency; water-lithium bromide absorption cooling; modular storage

1. Introduction

The energy consumption in buildings is an important issue, extensively emphasized in reported literature. Perez-Lombard et al. [1] published a review on the energy consumption of buildings and underlined that there is a trend regarding the growth in population, increased demand for comfort levels, increased time spent inside the building, and spread of the building sector that contributes to the increase of energy consumption, particularly related to HVAC (Heating, Ventilation and Air Conditioning) systems. The authors reported that 50% of the building consumption in the USA is due to HVAC systems. Also, in European Union (EU), the building consumption represents 37% of final energy, overpassing the transport and industry sectors. From this figure, 68% belongs to space conditioning of the residential sector. As this trend is maintained in the future, the authors conclude that among other priorities, energy efficiency and new technologies for producing energy should be considered for a sustainable energy future. On the same line, Sun et al. [2] have underlined the importance of methods proposed for reducing energy consumption in building heating and cooling, and conducted a study related to an evaluation of the inside temperature effect on thermal comfort and energy conservation. Marletta [3] studied the three most common air conditioning schemes and also a solar assisted one, outlining that thermally (solar) driven systems may be the most promising

answer to the energy-related problem. For these systems, some critical points have been emphasized, and among them, hot and/or cold storage is enumerated.

In this regard, the present paper is focused on the study of a single effect one-stage absorption cooling system (ACS), for which the thermal energy supplied to the vapor generator (desorber) is provided by a parabolic trough collector (PTC) and a fully mixed water storage tank (ST).

Among the most used ACS, the H_2O-LiBr one is preferred for buildings applications due to its advantages compared to other solar absorption cooling systems [4]. Some reported results for such systems are further discussed emphasizing systems requirements and the operation interval for covering the required cooling load.

Li et al. [5] proposed the use of a 56 m^2 PTC (26 m × 2.5 m) North-South oriented coupled to a 1 m^3 ST to drive a single-effect H_2O-LiBr absorption refrigeration system of a 23 kWp refrigeration capacity for a 102 m^2 room located in Kunming, China. Daily cooling coefficient of performance (COP) is reported to vary between 0.11 and 0.27. Experiments were performed between April and May 2014 and the system was turned on manually when stored hot water reached 65 °C and turned off at 40 °C. The wind speed varied between 2 and 5 m/s, influencing the PTC thermal efficiency. The variation of refrigeration power is plotted between noon and 7 pm, illustrating its variation between 20 kW at noon and 2 kW from 6 pm.

Mazloumi et al. [6] studied a 57.6 m^2 PTC associated with a hot water storage tank volume of 1.26 m^3 in Iran to cover a peak cooling load of 17.5 kW. The system operated between 6.49 h and 18.82 h (about 6:30 am to 7 pm).

Lu and Wang [7] compared a single effect H_2O-LiBr absorption cooling system used to cool water, coupled to a compound parabolic collector (CPC), with a double effect H_2O-LiBr absorption cooling system coupled to a PTC. For the first one, the authors reported 4 m^2 CPC/kW of cooling capacity and the system operated between 10 am and 4 pm, while for the second one, 2 m^2 PTC/kW of cooling capacity was noted and the operation interval was 2:30 pm to 5 pm. The authors recommended the second system due to its shortest payback year and high solar coefficient of performance.

Obviously, the operation time interval and the PTC and ST dimensions strongly depend on the climatic conditions for which the simulation is done. Solutions were further looked for in order to improve the whole system operation. Li and Sumathy [4] proposed using two hot storage units for solar heated single effect ACS, one proving 70–75% from the total heat input at a lower temperature (50–70 °C) and the other one proving the rest at a higher temperature (85–95 °C). The authors reported that this solution might increase the collected heat by a factor of 1.3–1.5 and decrease the collector area for cooling a building by 30–40%.

Other studies for maximizing performances of PTC-ACS systems are related to the heat transfer fluids and their mass flow rates. Bellos et al. [8] studied seven working fluids for a commercial PTC (Eurotrough ET-150) and optimized the mass flow rate for maximum PTC thermal and exergetic efficiencies. He reported pressurized water as the best fluid for low temperature applications, up to 550 K, and an optimum mass flow rate of 2 kg/s inside the PTC. Tzivanidis and Bellos [9] found an optimum specific mass flow rate of 0.03 kg/(s·m^2) from the point of view of a maximum achievable cooling load with a one stage H_2O-LiBr cooling system. They have considered a commercial PTC (PT1-IST) of 14 m^2 aperture and a 0.3 m^3 pressurized water ST. For a given coefficient of performance of the cooling module, expressed as vapor generator temperature dependence, they have determined the achievable cooling load. They reported a peak obtainable value of 3 kW for 8 h daily in Athena climatic conditions.

In the present study, the system is designed to cover the daily air conditioning cooling needs of a one-storey house located near Bucharest, Romania, having a living surface of 73.65 m^2 on the ground-floor and 59.05 m^2 on the first-floor. The subject was previously studied for the two most used pair-working fluids, namely NH_3-H_2O ACS [10] and H_2O-LiBr ACS [11], and the main problem encountered was related to the fact that the ACS operation is very sensitive to the storage tank water temperature feeding the vapor generator. For certain values of the PTC aperture and the water ST

capacity, either the ACS starts and stops too often, or it does not work at all in certain times of the day, due to the fact that the water temperature is either too low or too high. For a given PTC module, a lower ST capacity allows water to heat up enough in the morning so that ACS is turned on, but in the afternoon, its thermal capacity is undersized for the required cooling load, so the ACS is turned off. On the other hand, a larger ST would permit the ACS to remain turned on in the afternoon, but the water temperature would be too low in the first part of the day. Consequently, the ST capacity and the PTC dimensions should be carefully correlated in order to maintain an operating ACS for as long as possible. A narrow range of correlated dimensions was found and reported. For the given cooling load, of 4.7 kWp around 2 pm, the longest continuous operation was found to be from 9 am to 5:10 pm for the NH_3-H_2O cooling system using 10 m × 2.9 m PTC aperture with a 0.16 m^3 capacity water ST [10], and from 10:30 am to 6 pm for the H_2O-LiBr cooling system using 6 m × 2.9 m PTC aperture with a 0.22 m^3 water ST [11]. Because of the fact that the water is pressurized, it is important to emphasize that the quantity of water considered in computations was 160 kg and respectively, 220 kg. This instability was also studied by other authors. For example, Porumb et al. [12] reported that for the H_2O-LiBr system, temperatures in the desorber higher than 100 °C combined to condenser cooling fluid temperatures lower than 20 °C increase the risk of crystallization. This process is dangerous since the salt crystals could block the solution pipes. They also explained that lower desorber temperatures result in too low degassing zones and they recommend desorber temperature values between 85 °C and 95 °C.

A solution was further implemented in order to improve the whole system operation by maintaining the water temperature within the required interval for ACS operation [13]. Splitting the storage tank of 220 kg of water into two sub-tanks (one of 100 kg and the other one of 40 kg), the operation interval of the ACS was extended by about two hours daily in the studied case. The dimensions were selected by successive iterations, in order to cover the longest possible period of operation.

The only target for the previous reported studies was to maintain the ACS in operation as long as possible. The exergetic efficiency of the ACS module in this case varied throughout the simulation day between 0.1 and 0.22 for the NH_3-H_2O cooling system [10], and between 0.24 and 0.44 for the H_2O-LiBr cooling system [11], respectively.

In the present study, the target is to extend the working time period of the ACS operating at maximum exergetic efficiency for as long as possible. The proposed solution consists of splitting the storage tank into two modules, one which will feed the ACS desorber at optimum temperature and the second one which will play the role of a buffer for covering thermal needs when solar energy is insufficient. To emphasize the improvements achieved by implementing the proposed solution, a comparison with one volume storage tank system is performed.

2. System Description and Constraints

The considered solar driven system is shown in Figure 1. A parabolic trough collector (PTC) with a tubular receiver is used to catch solar radiation for heating water. The collector is fixed oriented at an East-West direction, facing South, and tilted at a fixed angle of 30° for the entire day. The tilt was considered from previous work regarding the optimum value for reaching maximum direct radiation at noon [14]. The hot pressurized water is stored in two fully mixed storage tanks, at temperatures T_{ST} and T_{ST2}, respectively. It is then used to provide the necessary heat load in the desorber of an absorption cooling system. As it is recirculated through the receiver tube of the PTC, its temperature increases from the storage tank temperature to T_{fo}, as an effect of the absorbed solar radiation, G_{Ab}. When exiting the receiver tube, the hot water returns to the storage tank, increasing the bulk temperature. A certain mass flow rate of main ST fluid leaves the tank and heats the H_2O-LiBr solution inside the desorber of the ACS, from state 2 to state 3, as shown in Figure 1. As heat is transferred from the main ST fluid to the H_2O-LiBr solution, the fluid temperature decreases to $T_{G,o}$ and returns the ST. On the other hand, pure H_2O vapors are leaving the desorber towards the cooling

part of the ACS. They condense in the air cooled condenser, are throttled in the throttling valve TV to state 5, and then evaporate during the air cooling process taking place in the evaporator where the cooling load is achieved. Entering the absorber as dry vapors at state 6, they absorb the throttled LiBr solution at state 8. The process is exothermic so that a heat rate is rejected to the ambient. The mixed solution leaves the absorber at state 1 and returns to the desorber.

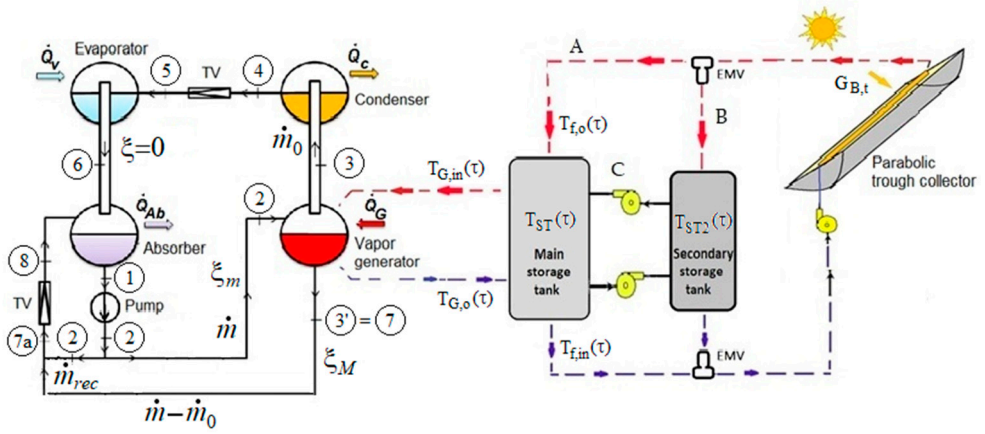

Figure 1. Architecture of the considered system.

With respect to the previous studied systems [10,13], the water heated inside the PTC might feed either entirely the main ST to increase the water temperature at the desired level, or entirely the secondary ST if the main ST temperature is satisfactory, or both of them at the same time. A temperature sensor installed on the main ST will control the electromagnetic valves EMV to open certain paths for the heat transfer fluid exiting the PTC. This temperature level is controlled in order to impose the ACS operation regime for maximum exergetic efficiency. Also, the main ST could be fed either from the PTC, from the secondary ST, or from both of them simultaneously when the solar energy is not sufficient. The heat input to the ACS desorber is only provided from the main ST.

The second system to which we compare the results has only one storage tank, so that no control on the water temperature is performed. In that case, the PTC feeds the one-volume ST, which feeds the ACS desorber. The system architecture is similar to the one presented in Figure 1, having no secondary storage tank.

The cooling load used here was previously computed for a two-storey house having a living surface of 73.65 m^2 on the ground-floor and 59.05 m^2 on the first-floor. Heat transfer processes through all building elements (exterior and interior walls, windows, doors, number of doors opening daily, number of occupants in time, etc.) were considered for an interior desired temperature of 22 °C. All details are available in paper [10]. The maximum values of the cooling load were met on 15 July and are presented in Figure 2. The peak value of 4.7 kW is reached at 2 pm. The entire system is intended for driving the ACS under this cooling load between 9 am and 6 pm.

The system operation is also constrained by the ambient characteristics, namely the exterior air temperature and available solar radiation. As in the previous studies, these values have been determined from databases of Meteonorm V7.1.8.29631 software [15], applying a time average between 1991 and 2010 for solar radiation and between 2000 and 2009 for ambient temperature. Their daily variation is presented in [10]. Solar radiation is available from 6 am to 7 pm and reaches a maximum value of about 900 W/m^2 at noon. Air temperature varies between 26 °C at 4 am and 38 °C at 4 pm. Note that the cooling load peak is shifted with respect to maximum solar radiation due to the thermal inertia of building elements.

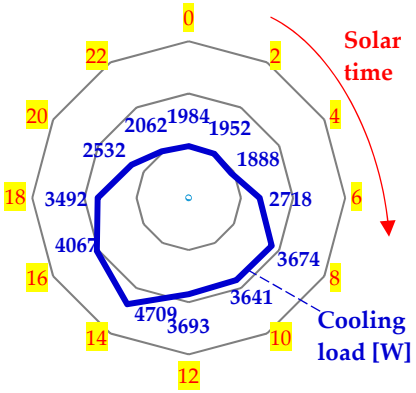

Figure 2. Cooling load, in *W*, versus solar time, on 15 July, for the studied house.

3. Flow Rates Control and Solving Algorithm

The flow rates control defines the operation strategy and only applies for the two modules ST system (Figure 1). It is thought to assure the operation of ACS at maximum exergetic efficiency. In the case of the one-volume ST system to which we compare it, no control is applied on the flow rates as the water is only recirculated through a single ST.

The parts of the considered system are activated turn by turn as follows. The PTC module is activated when solar radiation becomes available. In this case, water pumps are feeding the PTC tubes with water from the ST, and water is heated and returned to the ST. If no cooling load is applied, the water is just recirculated between PTC and ST and thermal energy is stored for later use. When a cooling load is applied, starting at 9 am, the hot water from the main ST feeds the ACS desorber and returns to the same ST. It is then heated by passing through the PTC and/or by mixing with hot water from the secondary ST. After 6 pm, the water is again recirculated only between PTC and ST, and heated as long as solar radiation is still available. After sunset, only losses to the ambient are occurring and the ST water temperature naturally drops.

To achieve the stated target, the first step is to complete an exergetic analysis of the cooling system and to determine the exergetic efficiency variation throughout the day as a function of possible desorber temperatures. The variable cooling load and ambient temperature will constrain each time-step ACS operation.

It was proved that the exergetic efficiency presents a maximum with respect to desorber temperature [16,17]. Thus, one might determine the desorber temperature value corresponding to maximum exergetic efficiency at each time-step, and consequently, the hot water temperature coming from the PTC-ST modules and feeding the ACS desorber.

The next step is to design the ST dimensions and to control the valves between PTC and ST so that the water inside the main ST will have the time-step optimum values determined above.

It is obvious that at system startup, and more precisely at PTC module startup, the valve from the PTC outlet will open to feed only the main ST (way A in Figure 1 will be activated). Afterwards, a temperature sensor opens the valve from the PTC outlet to feed the main ST (way A in Figure 1) only if the temperature inside it is lower than the optimum desired value. When the temperature reaches the optimum value, way A will close and way B will open so that hot water is stored in the secondary ST. Conversely, if the temperature in the main ST is at the optimum level or higher, the valve will only open way B and the PTC will entirely feed the secondary ST.

At the next level, the hot water from the main ST feeds the ACS desorber and returns the main ST with a lower temperature. If this temperature is under the next time-step optimum level, the PTC will feed the main ST by activating way A. If at any time the heat absorbed from the PTC fluid is insufficient to reach the optimum temperature value, the water in the main ST could be complementarily heated by stored water in the secondary ST, if its temperature level is higher, by activating way C. In this case, the necessary mass flow rate of water from the secondary ST is computed, so that the temperature of the water from the main ST attains the optimum value. After the heating process, the same quantity of water returns the secondary ST with a lower temperature.

The mass flow rate is kept constant through the PTC. When the PTC feeds only one storage tank, the same mass flow rate of water reenters the PTC at the temperature level from that ST, recalculated at the next time-step. When splitting between the two storage tanks, the mass flow rate of returning water to the PTC will have the temperature obtained from the adiabatic mixing of the two flow rates, each of them at the corresponding ST temperature.

All temperature computations are further detailed.

4. Mathematical Modelling

The mathematical modelling is separately presented for each system module.

4.1. Energetic Analysis and Exergetic Efficiency of the Cooling System

The single effect one stage H_2O-LiBr absorption cooling system is computed under an EES environment [18]. The cooling load is time dependent, as shown in Figure 2. The condensation and absorber temperatures, t_C and t_{Ab}, respectively, are also time dependent, constrained by the exterior air temperature t_a, so that $t_C = t_{Ab} = t_a + (2 \div 4\ ^\circ C)$. A constant vaporization temperature t_V of 10 °C is considered. All processing occurring inside the cooling module is represented in the enthalpy -concentration h-ξ diagram in Figure 3.

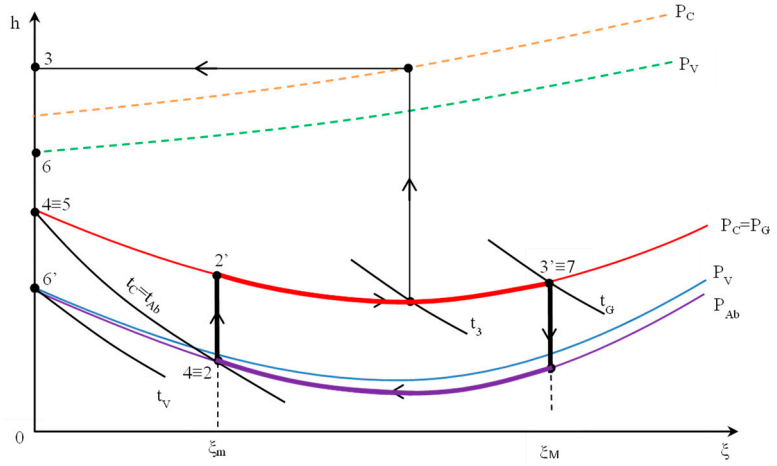

Figure 3. Enthalpy-concentration h-ξ diagram of H_2O-LiBr ACS (absorption cooling module).

At each time-step, a steady state operation of the ACS is assumed since the transient response of the ACS module is negligible in comparison to that of the storage tank.

The cooling cycle in solved by applying an SSCLiBr.dll external routine for each state, providing as input data three independent known parameters for each state, as specified in Table 1.

Table 1. State independent parameters of ACS (absorption cooling module).

State	State Description	Parameters
1	Low pressure saturated solution at the exit of the absorber, entering the liquid pump	t_C, p_{Ab}, saturated liquid at $t_1 = t_{Ab} = t_C$ $p_{Ab} = p_V - (0.08 \div 0.1)\ kPa$ $p_V = p_{sat}(H_2O, t_V)$
2	High pressure saturated solution at the exit of pump, entering the desorber (vapor generator)	p_C, h_2, $\xi_1 = \xi_2$, $p_C = p_{sat}(H_2O,\ t_C)$, $h_2 = h_1 - \frac{p_C - p_V}{\rho}$
3	Saturated vapor refrigerant at the exit of desorber, entering the condenser (pure water vapors) 2–3 desorbing process: 2′ boiling start; 3′ end of boiling process	t_3, $p_G = p_C$, $\xi_3 = 0$ $2'(\ p_G = p_C,\ \xi_{2'} = \xi_2,$ sat.liq.) $3'(p_G = p_c,\ t_{3'} = t_G,$ sat.liq.)
4	Subcooled liquid refrigerant at the outlet of condenser entering throttling valve (TV)	t_c, p_c, $\xi_4 = 0$
5	Low pressure humid vapor refrigerant at the exit of TV entering evaporator.	p_V, $\xi_5 = 0$, $h_5 = h_4$
6	Humid vapor refrigerant at the exit of evaporator, entering the absorber	p_V, $\xi_6 = 0$, $t_6 = t_v$
7	Diluted solution at the outlet of desorber, entering throttling valve (TV)	$7 \equiv 3'$
7a	Mixture of concentrated and diluted solution entering throttling valve	h_{7a}, $\xi_{7a} = 0$, $p_G = p_C$ [1]
8	Low pressure solution at the outlet of throttling valve, entering the absorber	$h_8 = h_{7a}$, $\xi_8 = \xi_{7a}$, p_{Ab}

[1] h_{7a}, ξ_{7a} are determined from mass and energy balance Equations (6) and (7).

In order to compute mass flow rates and heat rates for the ACS module, mass balance equations and energy balance equations are applied as follows:

- The mass flow rate of refrigerant is computed from the imposed cooling load:

$$\dot{m}_0 = \frac{\dot{Q}_V}{(h_6 - h_5)}. \tag{1}$$

- The mass flow rate of the diluted solution is determined as $\dot{m} = f \cdot \dot{m}_0$, in which the circulation ratio f is determined from the mass balance equation on the desorber:

$$\dot{m}\xi_2 = \dot{m}_0\xi_3 + (\dot{m} - \dot{m}_0)\xi_7 \tag{2}$$

in which ξ_2 represents the concentration of diluted solution (usually denoted by ξ_m), ξ_7 is the concentration of strong solution (usually denoted by ξ_M), and $\xi_3 = 0$, as specified in Table 1. It results that:

$$f = \frac{\xi_M}{\xi_M - \xi_m} \tag{3}$$

- The mass flow rate of recirculated solution inside the absorber is computed as:

$$\dot{m}_{rec} = a \cdot \dot{m}_0 \tag{4}$$

where $a = 15 \div 50$ is the recommended recirculation factor for a good operation [19–21]. Osta-Omar and Micallef [22] proposed an ACS with an adiabatic absorber in which the solution is recirculated without passing the throttling valve and defined the recirculation factor as the

mass of solution $\dot{m}$. (instead of mass of refrigerant $\dot{m}_0$). The authors considered its value to be 25. Nevertheless, most of the reported papers in the literature consider no recirculation. This complementary process is applied in the case of crystallization risk, to dilute the solution. As explained by Osta-Omar and Micallef [23], the critical point in which crystallization tends to occur is in the weak solution between the throttling valve and the absorber since the solution is characterized here by a dangerous combination of the lowest temperature and the highest concentration; crystallization of a salt takes place if the temperature of a saturated solution drops. For the present numerical simulation, we considered the case with no recirculation ($a = 0$), but we have verified the crystallization absence at each time step.

- The mass flow rate of solution at the absorber outlet should be:

$$\dot{m}_{Ab} = \left(\dot{m} + \dot{m}_{rec}\right) \Rightarrow \dot{m}_{Ab} = (f + a)\dot{m}_0 \tag{5}$$

For determining the properties of state 7a, a mass balance equation when mixing streams 2 and 7 for the inlet to the throttling valve is applied:

$$\left(\dot{m}_{Ab} - \dot{m}_{rec} - \dot{m}_0\right)\xi_7 + \dot{m}_{rec}\xi_2 = \left(\dot{m}_{Ab} - \dot{m}_0\right)\xi_{7a} \tag{6}$$

and accordingly the energy balance equation:

$$\left(\dot{m}_{Ab} - \dot{m}_{rec} - \dot{m}_0\right)h_7 + \dot{m}_{rec}h_2 = \left(\dot{m}_{Ab} - \dot{m}_0\right)h_{7a}. \tag{7}$$

Applying the energy balance equation to the condenser, absorber, desorber, and solution pump, one determines the energy rates presented in Table 2.

Table 2. Energy rates of the ACS determined from energy balance equations.

Component	Thermal Load
Condenser	$\dot{Q}_C = \dot{m}_0(h_4 - h_3)$
Evaporator	$\dot{Q}_V = \dot{m}_0(h_6 - h_5)$
Desorber	$\dot{Q}_G = \dot{m}_0[f(h_7 - h_2) + (h_3 - h_7)]$
Absorber	$\dot{Q}_{Ab} = -\dot{m}_0[h_6 - h_8 + (f + a)(h_1 - h_8)]$
Solution pump	$\dot{W}_P = \dot{m}_{Ab}\lvert w_p\rvert = (f + a)\dot{m}_0\lvert w_p\rvert = (f + a)\dot{m}_0(h_2 - h_1)$

The overall coefficient of performance and exergetic efficiency are:

$$COP = \frac{\dot{Q}_V}{\dot{Q}_G + \dot{W}_P};\ \eta_{ex} = \frac{Ex(\dot{Q}_V)}{Ex\left(\dot{Q}_G\right) + \dot{W}_P} \tag{8}$$

where

$$Ex\left(\dot{Q}_V\right) = -\dot{Q}_V\left(1 - \frac{T_a}{T_V}\right);\ Ex\left(\dot{Q}_G\right) = \dot{Q}_G\left(1 - \frac{T_a}{T_{Gmed}}\right) \tag{9}$$

in which T_{Gmed} is a mean value for the generator temperature, defined as the arithmetic mean between temperature values of the states corresponding to the beginning and end of the desorbing process $T_{Gmed} = \frac{T_{2'} + T_{3'}}{2}$.

At each time-step, numerical results are checked for physical meaning and system correct operation. Thus, the first law and second law of thermodynamics are checked, and also the operation above the crystallization line. The crystallization is avoided if the solution temperature in critical points 7 and 8 is above the crystallization limit.

4.2. Parabolic Trough Collector

A parabolic trough collector with a tubular receiver is chosen for the simulation. Its characteristics are described by the following parameters: aperture width H_{PTC}; length L_{PTC}; optical efficiency η_{opt}; pipe interior and exterior diameters D_{pi} and D_{pe}, respectively; tubular glass cover interior and exterior diameters $D_{gls,I}$ and $D_{gls,e}$, respectively; mass flow rate of fluid inside the tube $\dot{m}_f$; glass properties (absorptivity α_{gls}, emissivity ε_{gls}, transmittance τ_{gls}); and pipe properties (absorptivity α_p, emissivity ε_p).

Two commercial PTC are selected, recommended for applications up to 250 °C [24], for whom the numerical data given in Table 3 were employed.

Table 3. Numerical data for the PTC (parabolic trough collector) used [9,24,25].

Parameter	PT1-IST		PTC1800 Solitem	
	Value	Unit	Value	Unit
$H_{PTC} \times L_{PTC}$	2.3 × 6.1	m	1.8 × 5.09	m
η_{opt}	0.7625	-	0.7	-
D_{pi}/D_{pe}	47/51	mm	35.50/38	mm
$D_{gls,i}/D_{gls,e}$	71/75	mm	60.6/65	mm

For the glass and tube properties, in both cases, the following values have been used: α_{gls} = 0.02, ε_{gls} = 0.88, τ_{gls} = 0.95, α_p = 0.96, ε_p = 0.000327·T_{pi} − 0.065971 [26] function on pipe interior wall temperature T_{pi}. The mass flow rate of water inside the tube was set to 0.07 kg/s.

The mathematical model of PTC consists of applying the energy balance equations on the inner and outer surfaces of the absorber pipe and glass cover, respectively. It is detailed in the previous study [10]. In Figure 4, the heat rates have been depicted as they are exchanged at the glass cover and receiver pipe, and transmitted to the fluid.

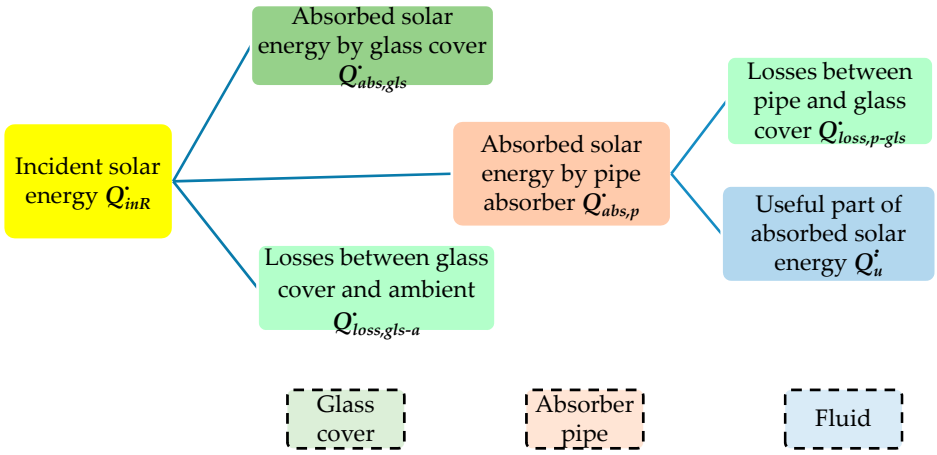

Figure 4. Heat rates associated with PTC (parabolic trough collector).

Briefly, the incident solar energy is computed according to [27] from the incident solar radiation density G_{Bt} on the tilted aperture that is extracted from Meteonorm software:

$$\dot{Q}_{in,R} = \eta_{opt} H_{PTC} L_{PTC} G_{Bt} \tag{10}$$

Part of $\dot{Q}_{in,R}$ is lost to the ambient on the glass outer surface:

$$\dot{Q}_{loss,gls-a} = \pi D_{gls,e} L_{PTC} h_w \left(T_{gls,e} - T_a\right) + \pi D_{gls,e} L_{PTC} \varepsilon_{gls} \sigma \left(T_{gls,e}^4 - T_{sky}^4\right) \tag{11}$$

while the rest is absorbed by the glass

$$\dot{Q}_{abs,gls} = \alpha_{gls}\dot{Q}_{in,R} \tag{12}$$

and by the pipe:

$$\dot{Q}_{abs,p} = \tau_{gls}\alpha_p\dot{Q}_{in,R} \tag{13}$$

The convection heat transfer coefficient due to wind h_w is equal to 6.46 W/(m^{2}K), computed for a wind speed of 0.2 m/s [28].

The heat rate absorbed by the pipe, $\dot{Q}_{abs,p}$, is partially lost through radiation back to the glass

$$\dot{Q}_{loss,p-gls} = \pi D_{pe} L_{PTC}\sigma \frac{T_{pe}^4 - T_{gls,i}^4}{\frac{1}{\varepsilon_p} + \frac{1-\varepsilon_{gls}}{\varepsilon_{gls}}\frac{D_{pe}}{D_{gls,i}}} \tag{14}$$

and the rest in transmitted to the heat transfer fluid inside the pipe, by convection:

$$\dot{Q}_u = \pi D_{pi} L_{PTC} h_f \left(T_{pi} - T_f\right); \dot{Q}_u = \dot{m}_f c_{p,f}\left(T_{fo} - T_{fi}\right) \tag{15}$$

The convection heat transfer coefficient h_f is computed from the Nusselt number as follows:

$$h_f = \frac{Nu_f \lambda_f}{D_{pi}}; Nu_f = \begin{cases} 4.36, \ for\ laminar\ flow \\ 0.023 Re_f^{0.8} Pr_f^{0.4}, \ for\ turbulent\ flow \end{cases} \tag{16}$$

The flow regime is determined at each time-step, based on the constant mass flow rate of water inside the pipe and temperature dependent properties used for computing Reynolds and Prandtl numbers, *Re* and *Pr*, respectively.

In this set of equations, $T_{gls,e}$, $T_{gls,i}$, T_{pe}, T_{pi}, and T_f represent the glass, pipe, and fluid mean temperatures, respectively, while T_{fo} is the PTC outlet fluid temperature. All of them are unknown. The inlet fluid temperature T_{fi} is known and is equal to the main storage tank temperature T_{ST}. At each time-step, the equations are solved, all temperatures determined, and the outlet fluid temperature T_{fo} is further used as the input to the storage tank at the next time-step.

4.3. Storage Tank Modules

The first simulation was done for the system with one volume storage tank. The capacity was chosen by successive iterations in order to obtain the longest possible ACS operation with the given PTC module. Namely, when coupling the PT1-IST module, a capacity of m_{ST} = 170 kg was selected. For the second choice, Solitem PTC1800, two modules of PTC are required and consequently, the ST capacity is m_{ST} = 275 kg.

A constant heat loss coefficient is assumed and computed from the $(UA)_{ST}$ = 5 W/K value, recommended in the literature (UA = 1.7 ÷ 11 W/K) [29]. By applying the mathematical expression of the first law, one obtains the following ordinary differential equation:

$$\left(mc_p\right)_{ST}\frac{dT_{ST}}{d\tau} = \dot{Q}_u - \dot{Q}_G - (UA)_{ST}(T_{ST} - T_a) \tag{17}$$

that is integrated in the time-step interval in order to compute the storage tank temperature at the next time-step (n + 1) based on the value from the previous time-step (n):

$$T_{ST}^{(n+1)} = T_{ST}^{(n)} + \frac{\left[\dot{Q}_u^{(n)} - \dot{Q}_G^{(n)} - (UA)_{ST}\left(T_{ST}^{(n)} - T_a^{(n)}\right)\right]\Delta\tau}{\left(mc_p\right)_{ST}} \tag{18}$$

The time-step $\Delta\tau$ set for the simulations is 10 min for the whole day.

For the simulations done with two storage tank modules, the computations are split by cases of operation, as follows:

1. When the PTC is not started, the two ST temperatures are computed as follows:

$$T_{ST}^{(n+1)} = T_{ST}^{(n)} + \frac{\left[-\dot{Q}_G^{(n)} - (UA)_{ST}\left(T_{ST}^{(n)} - T_a^{(n)}\right)\right]\Delta\tau}{(mc_p)_{ST}} \tag{19}$$

for the main ST module, and, respectively, for the secondary ST module:

$$T_{ST2}^{(n+1)} = T_{ST2}^{(n)} + \frac{\left[-(UA)_{ST2}\left(T_{ST2}^{(n)} - T_a^{(n)}\right)\right]\Delta\tau}{(mc_p)_{ST2}} \tag{20}$$

The difference between the two relations consists of the fact that the main ST might feed the desorber of the ACS, thus we notice in its calculation the term corresponding to $\dot{Q}_G^{(n)}$. The useful heat rate $\dot{Q}_u^{(n)}$ does not appear, as the PTC is turned off. The secondary ST only loses heat to the ambient.

2. When the PTC is on and the main ST temperature is less than the optimum desired temperature (determined for maximum exergetic efficiency as presented in Section 4.1), the PTC might feed either entirely the main ST, or both ST modules. The following subcases are possible:

   - The main ST is firstly fed from the PTC. If its temperature becomes higher than the optimum one, than the temperature sensor will close the valve towards the main ST and will open the way towards the secondary one. In this way, the main ST temperature reaches the optimum value and the rest of the available heat from the PTC is stored in the secondary ST. The two temperatures are computed as follows:

$$T_{ST}^{(n+1)} = T_{ST,opt}^{(n+1)} \tag{21}$$

$$T_{ST2}^{(n+1)} = T_{ST2}^{(n)} + \frac{\left[\left(\dot{Q}_u^{(n)} - \dot{Q}_{uST1}^{(n)}\right) - (UA)_{ST2}\left(T_{ST2}^{(n)} - T_a^{(n)}\right)\right]\Delta\tau}{(mc_p)_{ST2}} \tag{22}$$

   where the term $\dot{Q}_{uST1}^{(n)}$ denotes the heat rate transferred from the PTC to the main ST and is computed as:

$$\dot{Q}_{uST1}^{(n)} = \frac{\left(T_{ST,opt}^{(n+1)} - T_{ST}^{(n)}\right)(mc_p)_{ST2}}{\Delta\tau} + \dot{Q}_G^{(n)} + (UA)_{ST}\left(T_{ST}^{(n)} - T_a^{(n)}\right) \tag{23}$$

   - If the main ST temperature is still less than the optimum one after heating from the PTC, a check is performed for the secondary ST to verify if complementary thermal energy is stored and can be used.

If the secondary ST temperature is lower than the main ST one, there is no stored thermal energy available at this time-step. Thus, the main ST temperature is computed by Equation (18), while for the secondary ST, one Equation (20) is applied.

Otherwise, stored thermal energy is available for use. In this case, the main ST was fed from the PTC and is complementarily fed from the secondary ST. One needs to compute the necessary

mass flow rate of circulated water between the two ST modules. As the target is to bring $T_{ST}^{(n+1)}$ at the optimum value $T_{ST,opt}^{(n+1)}$, the necessary mass flow rate is:

$$\dot{m}_{R2} = \frac{\frac{(mc_p)_{ST}\left(T_{ST,opt}^{(n+1)} - T_{ST}^{(n)}\right)}{\Delta\tau} - \dot{Q}_u^{(n)} + \dot{Q}_G^{(n)} + (UA)_{ST}\left(T_{ST}^{(n)} - T_a^{(n)}\right)}{c_{p,ST2}T_{ST2}^{(n)} - c_{p,ST}T_{ST,opt}^{(n+1)}} \tag{24}$$

If the corresponding mass quantity is available inside the secondary ST, then $T_{ST}^{(n+1)} = T_{ST,opt}^{(n+1)}$ and the temperature of the secondary ST becomes:

$$T_{ST2}^{(n+1)} = T_{ST2}^{(n)} + \frac{\left[-(UA)_{ST2}\left(T_{ST2}^{(n)} - T_a^{(n)}\right) - \dot{m}_{R2}c_{p,ST2}T_{ST2}^{(n)} - c_{p,ST}T_{ST}^{(n+1)}\right]\Delta\tau}{(mc_p)_{ST2}} \tag{25}$$

Otherwise, the maximum available mass quantity existing in the secondary ST is used and the temperatures are:

$$T_{ST}^{(n+1)} = T_{ST}^{(n)} + \frac{\left[\dot{Q}_u^{(n)} - \dot{Q}_G^{(n)} - (UA)_{ST}\left(T_{ST}^{(n)} - T_a^{(n)}\right)\right]\Delta\tau + m_{ST2}\left(c_{p,ST2}T_{ST2}^{(n)} - c_{p,ST}T_{ST}^{(n+1)}\right)}{(mc_p)_{ST}} \tag{26}$$

$$T_{ST2}^{(n+1)} = T_{ST2}^{(n)} + \frac{\left[-(UA)_{ST2}\left(T_{ST2}^{(n)} - T_a^{(n)}\right)\right]\Delta\tau - m_{ST2}\left(c_{p,ST2}T_{ST2}^{(n)} - c_{p,ST}T_{ST}^{(n+1)}\right)}{(mc_p)_{ST2}} \tag{27}$$

Both last equations are solved for the two unknowns $T_{ST}^{(n+1)}$ and $T_{ST2}^{(n+1)}$.

3. When the PTC is on, but the main ST temperature is higher than the optimum desired temperature, the PTC will feed entirely the secondary ST:

$$T_{ST2}^{(n+1)} = T_{ST2}^{(n)} + \frac{\left[\dot{Q}_u^{(n)} - (UA)_{ST2}\left(T_{ST2}^{(n)} - T_a^{(n)}\right)\right]\Delta\tau}{(mc_p)_{ST2}} \tag{28}$$

In this case, the main ST temperature is computed with Equation (19).

5. Results and Discussion

All the equations above have been implemented in an EES environment, creating a subprogram for each system module and for input data that are read from outside, and calling them turn by turn in the main program. Firstly, Meteonorm data and computed cooling load are read. Afterwards, the PTC module is called for an initial ST temperature 10 °C higher than the ambient one. The output from the PTC is the outlet fluid temperature T_{f0} that becomes the input for the ST module. When the ST module is called, the cases presented in Section 4.3 are verified and consequently the new entries for the next time-step ACS and PTC calls are computed, $T_{ST}^{(n+1)}$ and $T_{ST2}^{(n+1)}$. The computations continue at the next time-step.

The ACS module is used twice at each computing time. Firstly, it is called to determine the desorber temperature T_G corresponding to the maximum exergetic efficiency. This is performed by a sensitivity study with respect to possible desorber temperatures T_G. The value corresponding to maximum exergetic efficiency is aimed to be maintained in the main storage tank. Secondly, it is called to compute ACS parameters and performances with T_G as the input parameter linked to the main ST achieved temperature.

The start computing time is midnight and the simulation is performed for 24 h.

The results are presented in what follows, for the two considered main case studies: one-volume storage tank and modular storage tank, respectively. As stated previously, an operating strategy of maximum ACS exergetic efficiency is applied in the second case. Both cases are simulated for the two commercial PTC presented in Section 4.2. The summary of studied cases is shown in Table 4.

Table 4. Summary of studied cases.

Storage Tank Type	PTC Type	Operation Strategy
One volume ST	PT1-IST	-
	PTC1800	-
Two modules ST	PT1-IST	$\eta_{Ex,max,ACS}$
	PTC1800	$\eta_{Ex,max,ACS}$

5.1. One-Volume Storage Tank Case

As presented in our previous studies [11,13], when the system is provided with a one-volume storage tank, a difficulty is encountered in finding the most appropriate dimensions of PTC-ST modules for the longest possible operation of the ACS.

5.1.1. PT1-IST Module with One-Volume ST

By successive iterations, when choosing the first PTC module, the PT1-IST one, the best results are obtained for an ST capacity of 170 kg. The results are shown in Figures 5–7. The maximum storage tank temperature reaches 108 °C at 2:30 pm, as presented in Figure 5. The longest continuous operation of the ACS module is between 11:10 am to 4:50 pm, revealed in Figure 6 by the "ACS on" plot. A lower capacity ST is not able to maintain the ACS operation in the afternoon, while a higher capacity results in a lower water temperature, consequently turning off the ACS module.

As presented in Figure 7, the *COP* varies throughout the day starting from a value of 0.5 at 11:10 am, reaches a maximum of 0.64 around 2 pm, and decreases to 0.32 at the ACS stop time. Similarly, the exergetic efficiency of the ACS is 0.37 at 11:10 am, reaches its maximum value of 0.43, and decreases to 0.25 at the ACS turn off time.

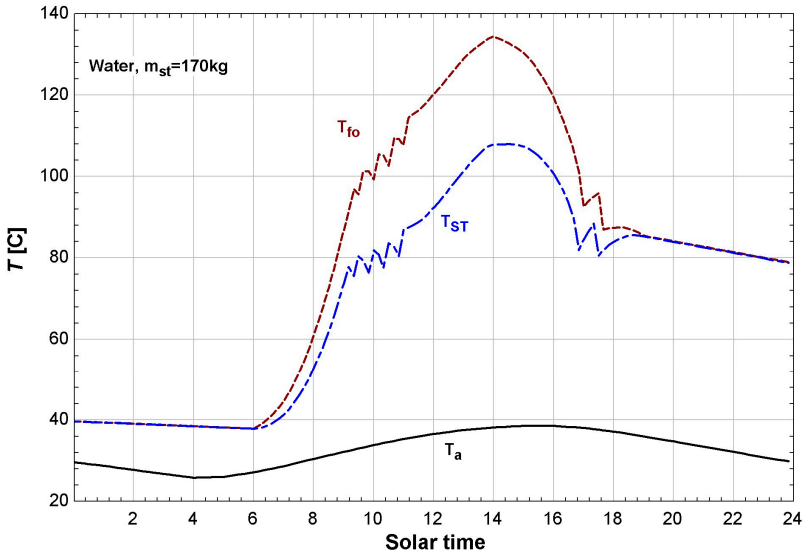

Figure 5. PTC outlet fluid and ST (storage tank) water temperatures for PT1-IST and 170 kg ST.

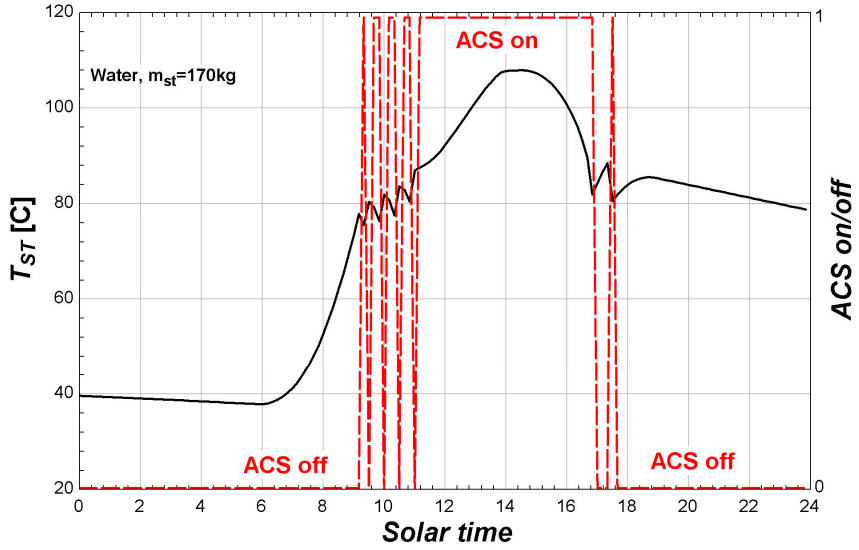

Figure 6. Storage tank water temperature and corresponding on/off ACS operating times for PT1-IST and 170 kg ST.

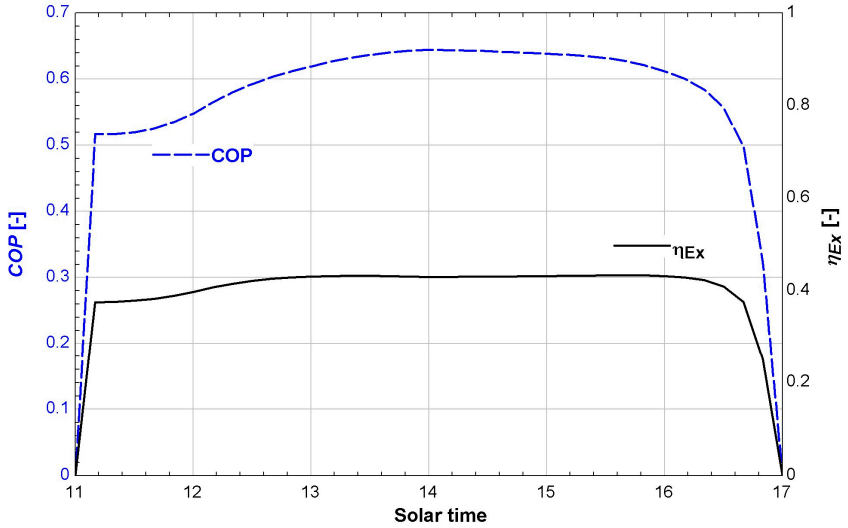

Figure 7. Coefficient of performance (*COP*) and exergetic efficiency (η_{Ex}) for ACS operating time, for PT1-IST and 170 kg ST.

As one may notice from Figure 6, the storage tank temperature has not increased sufficiently in the morning to keep the ACS on. One idea for improving its operation is to consider the water preheated from the previous operation day, so that at ACS theoretical start-up (9 am), there is sufficient thermal energy stored in the ST to feed the ACS desorber. Different preheat degrees have been applied, but with unsatisfactory results.

A preheat of 60 °C resulted in an ACS continuous operation from 9 am to 2 pm, as plotted in Figure 8a. After 2 pm, the water temperature increased dramatically so that the entire system is turned off as a safety measure, as the vaporization water temperature level in the solar collector was overpassed. A heat dissipation system could be used starting from 2 pm to avoid increasing the water temperature over 110 °C. This case would be similar to the result presented in Figure 6, where at the same time, the water temperature reached this maximum allowable level. As revealed, the operation of the absorption chiller covers the cooling period until 5 pm. In conclusion, a heat dissipation system

would extend the ACS operation interval, but would not cover the entire targeted one, since the cooling peak appears in the afternoon, simultaneously with decreasing solar radiation.

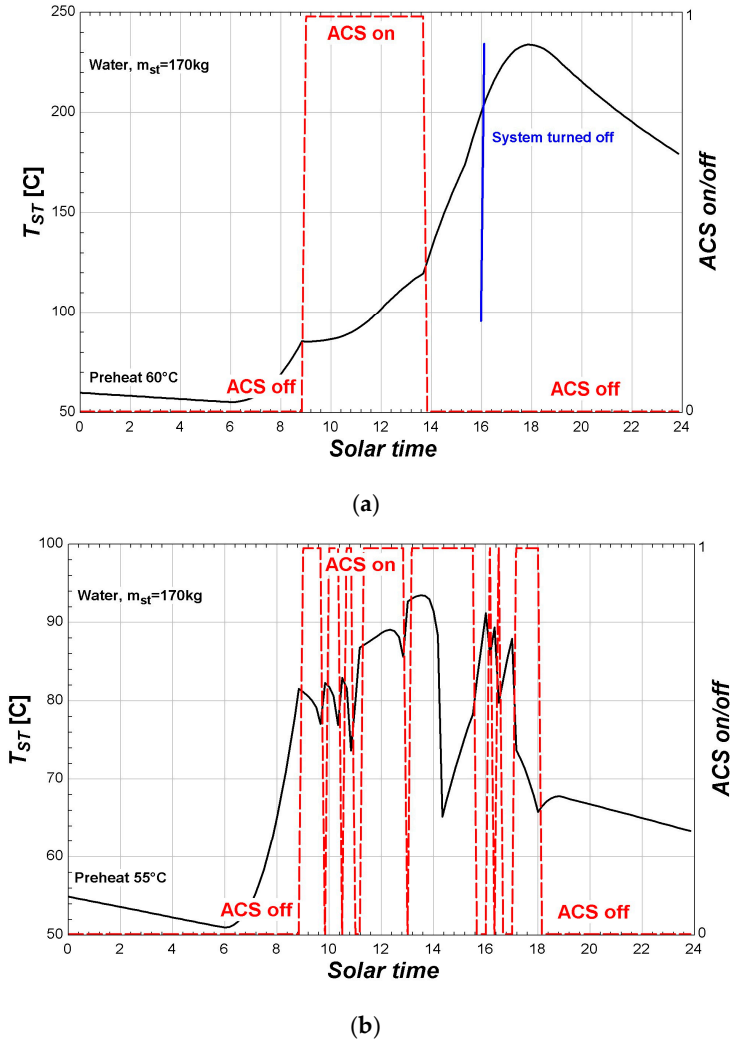

Figure 8. Storage tank water temperature and on/off ACS operating times for PT1-IST and 170 kg ST, with a preheat degree of (**a**) 60 °C; (**b**) 55 °C.

If a lower preheat is applied, 55 °C, the system starts early, but not for a long time. The operation is even worse, as seen in Figure 8b.

One concludes that when using the PT1-IST module, the temperature in the ST is too low in the morning. Preheat does not help, and neither does changing the ST capacity, and consequently, one may think about using a larger PTC.

5.1.2. PTC1800 Module with One-Volume ST

When selecting the Solitem PTC1800, two modules coupled in series are necessary, as the aperture area of one module is too small. The results are presented in Figure 9 and are similar to those obtained for the PT1-IST module. Since two modules result in a larger total aperture area, a higher capacity ST is required. The most appropriate value is found to be 275 kg. In this case, the continuous operating time interval is between 10:40 am and 6 pm, which is larger than in the first case. Again, the temperature is not sufficiently high to sustain the ACS operation in the morning, and preheating does not help. Different preheat degrees were tested, but without any considerable improvement. More than that, the

end-day ST temperature is about 88 °C and a simulation for the second day results in the ACS being off most of the time caused by the too high water temperature feeding the ACS desorber.

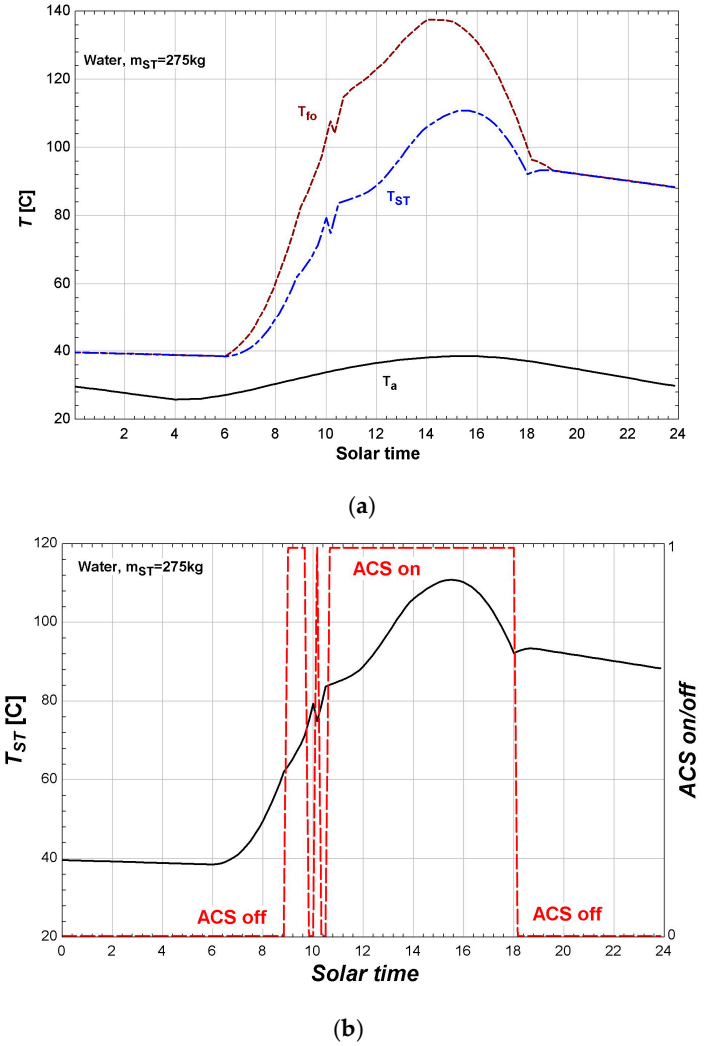

Figure 9. PTC outlet fluid and ST water temperatures (**a**) and on/off ACS operating times (**b**) for two PTC1800 modules and 275 kg ST.

One may conclude that the one-volume storage tank solution limits the ACS operation. When analyzing all the above results, one may see that the ST water temperature is either too low or too high to sustain the ACS operation. Thus, a possible improvement is to split the ST into two modules and to control the temperature in the module that feeds the ACS desorber.

5.2. Modular Storage Tank Case

The main storage tank is the one that feeds the ACS desorber. Its temperature is controlled and maintained in a suitable range for the ACS operation. The criterion is chosen to be the maximum exergetic efficiency of the ACS module.

In Figure 10a, one may see the ACS exergetic efficiency variation throughout the simulation day, for different possible desorber temperatures T_G. As the ambient temperature T_a and refrigerating load $\dot{Q}_V$ are time dependent, the exergetic efficiency has different variation profiles throughout the day. At each time-step, the maximum value was extracted and also the corresponding desorber temperature.

These optimum values are plotted in Figure 10b. The temperature found becomes a target for the main storage tank water temperature and thus it is denoted by $T_{ST,opt}$.

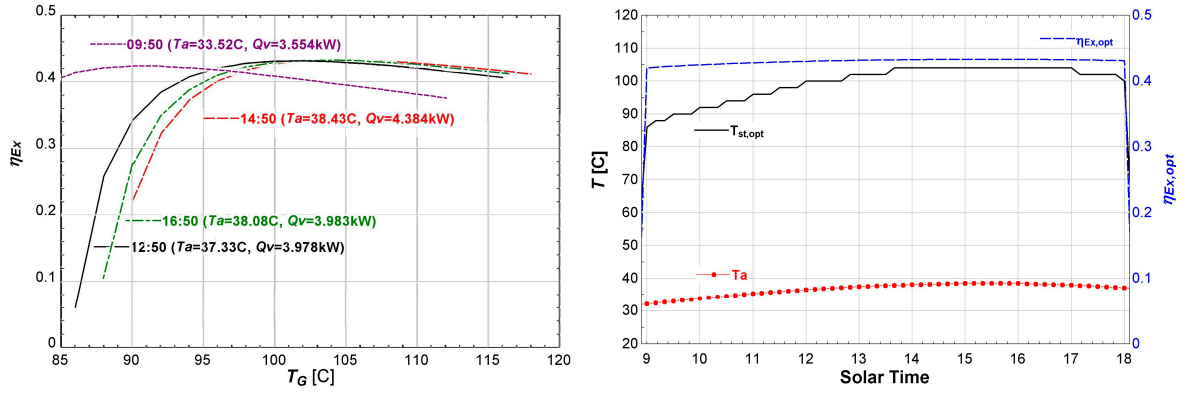

(**a**) (**b**)

Figure 10. (**a**) ACS Exergetic efficiency at different solar times, function on desorber temperature T_G; (**b**) Maximum exergetic efficiency $\eta_{Ex,opt}$ and optimum corresponding desorber/storage tank water temperature $T_{st,opt} = T_G$.

The temperature is controlled as explained in Section 4.3. By successive iterations, as applied above, the most appropriate ST dimensions are determined.

5.2.1. PT1-IST Module with Modular ST

When the PT1-IST module is selected, the best choice for the two ST modules is a main ST of 90 kg water and a secondary one of 90 kg water. This solution maintains the ACS in operation the longest and reveals the results presented in Figures 11 and 12. With respect to the previous case described in Section 5.1.1, the temperature of the water in the main ST is maintained as close as possible to the optimum desired values, here around 100 °C. The complementary thermal energy available from the PTC is stored in the secondary ST, as emphasized by the increase of its water temperature T_{ST2} in Figure 11a. The outlet fluid temperature from the PTC, T_{fo}, varies as the input temperature differs accordingly to the ST module that was fed from the PTC. At about 4 pm, both ST water temperatures drop and the ACS module is turned off, as one may see in Figure 11b.

By maintaining the main ST water temperature as close as possible to the optimum value (Figure 12a), a higher *COP* and exergetic efficiency for a longer time are obtained, as Figure 12b reveals.

One may conclude that an improvement was detected in the ACS operation, but a further solution is needed in order to extend the operation interval in the afternoon.

As the main ST water temperature dictates the ACS operation, a sensitivity study was performed with respect to its capacity. In Figure 13, one may see that lowering or increasing its capacity results in a lower operation interval. The ACS is stopped because one of the operating conditions is not fulfilled. When increasing the main tank capacity, an unusual variation of the time off is emphasized. In the case of 100–90 kg ST capacities, the operation time interval is shorter compared to the pair 110–90 kg. This is caused by the fact that at the turn-off time, the combination of the storage tank temperature (87 °C) and condensation one (38 °C) for the case 100–90 kg leads to an unfavorable degassing interval (defined as the difference between strong and weak solution concentrations). At this moment, the water recirculation from ST2 is required, but its temperature level is insufficient to sustain a continuous operation. In the case of 110–90 kg ST capacities, the temperature in the main ST is 103 °C and the combination to the same ambient temperature allows the system to operate. Its thermal capacity is larger and thus sustained the ACS operation without recirculation in comparison to the pair 100–90 kg. By comparison, when the main ST has a capacity of 90 kg, the water temperature is slightly higher and

also sustains the ACS operation better than in the case of 100–90 kg. It is all about a combination of the main ST water temperature, the condensation one (imposed by the ambient), and the cooling load at each time step.

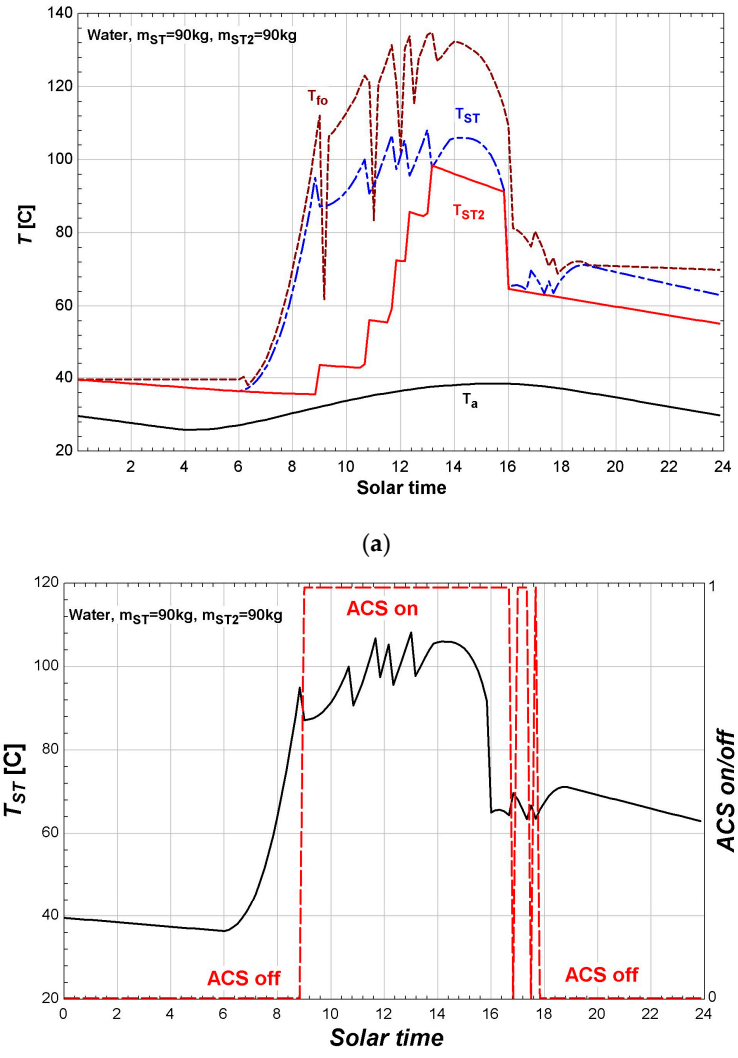

Figure 11. PTC temperatures (**a**) and on/off ACS operating times (**b**) for PT1-IST and 90 kg main ST and 90 kg secondary ST, respectively.

After performing a second sensitivity study with respect to the secondary ST capacity and without finding a better result, the conclusion drawn was that the two associated ST capacities of 90 kg are the best choice for this PTC module.

As one may see, the use of PT1-IST does not ensure a sufficiently high temperature inside the storage tanks to cover the ACS load in the afternoon. Thus, one needs a larger PTC. From the commercially available PTC modules, PTC1800 was selected. Again, as in the previous case, two modules will be connected in series.

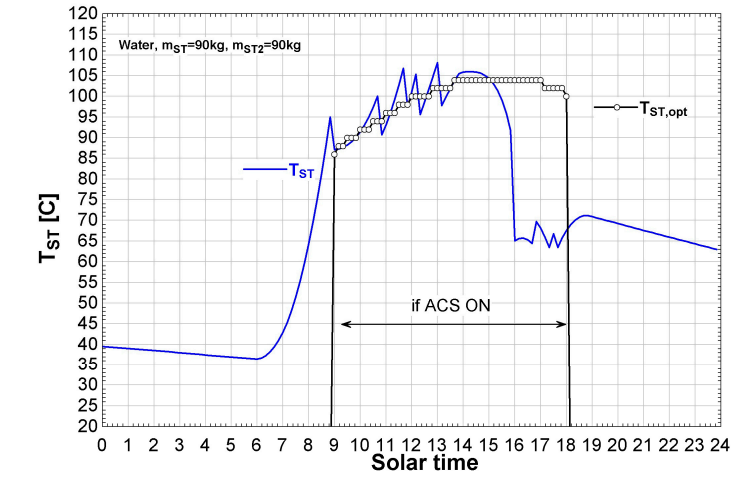

(**a**)

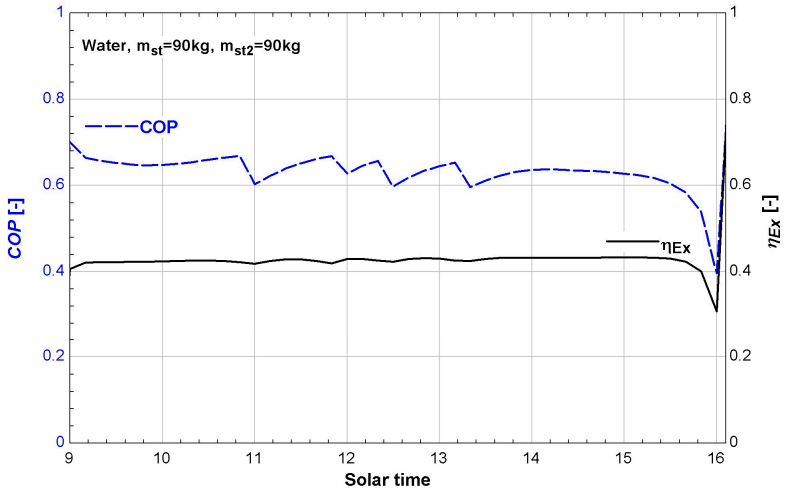

(**b**)

Figure 12. Achieved versus optimum main ST water temperature (**a**) and COP and ACS exergetic efficiency (**b**) for PT1-IST and 90 kg main ST + 90 kg secondary ST, respectively.

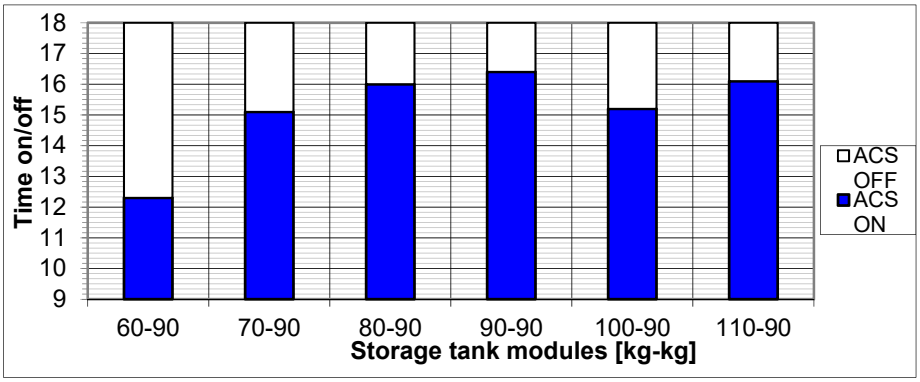

Figure 13. ACS operating time intervals; sensitivity with respect to main ST capacity, for PT1-IST and 90 kg secondary ST.

5.2.2. PTC1800 Module with Modular ST

By performing the same iterative procedure, the best solution is to attach to this PTC module two STs with capacities of 90 and 140 kg, respectively. The results emphasize that the water temperature inside the main storage tank is maintained all day at a quite constant value (Figure 14a), while the water temperature in the secondary ST increases more than in the first case presented in Section 5.1.2, due to the use of a larger aperture PTC. Consequently, the stored thermal energy in the secondary ST is better used and sufficient to keep the ACS module turned on all day, as one may see in Figure 14b.

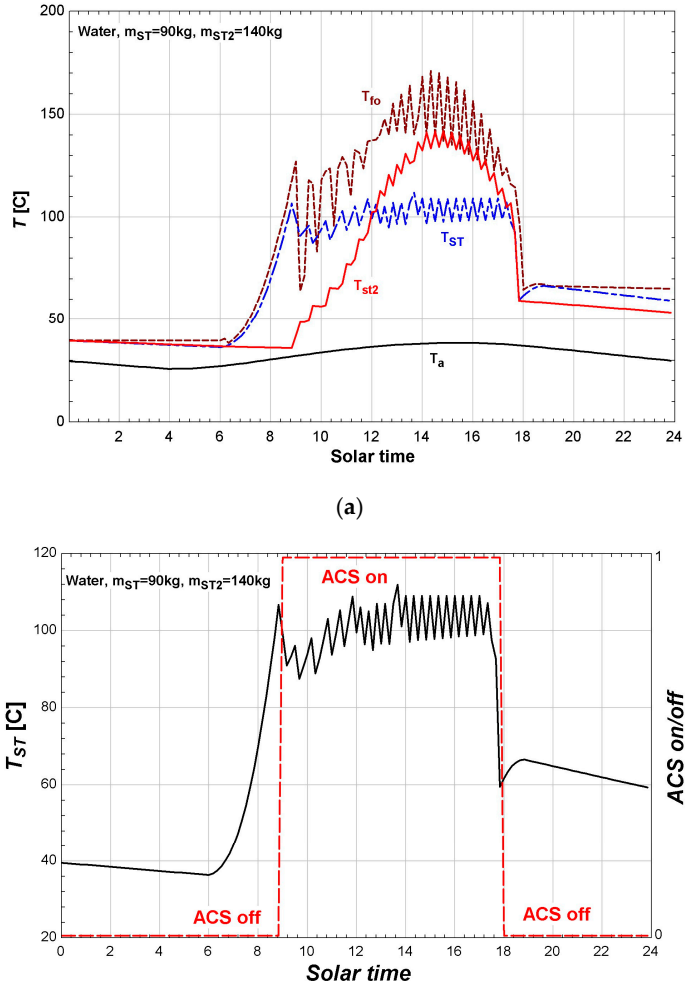

Figure 14. PTC outlet fluid and STs water temperatures (**a**) and on/off ACS operating times (**b**) for PTC1800 and 90 kg main ST + 140 kg secondary ST, respectively.

In Figure 15, one may see that the main ST water temperature is close to the optimum value all day long (Figure 15a), and thus the ACS module operates at an exergetic efficiency close to the maximum one (Figure 15b).

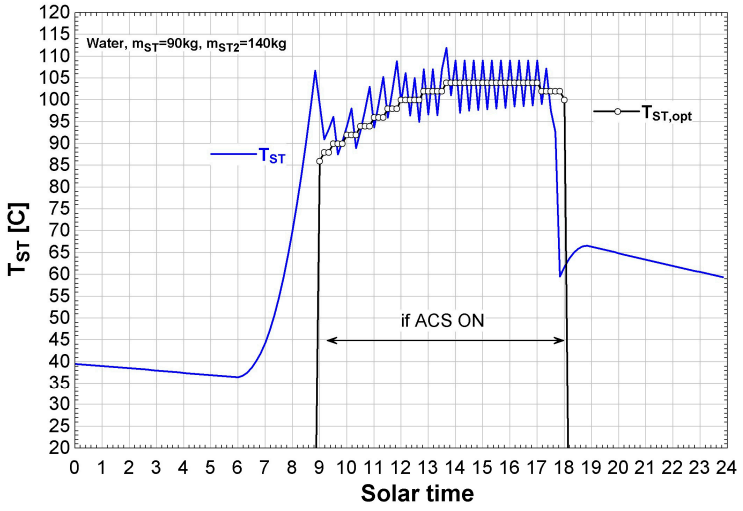

(**a**)

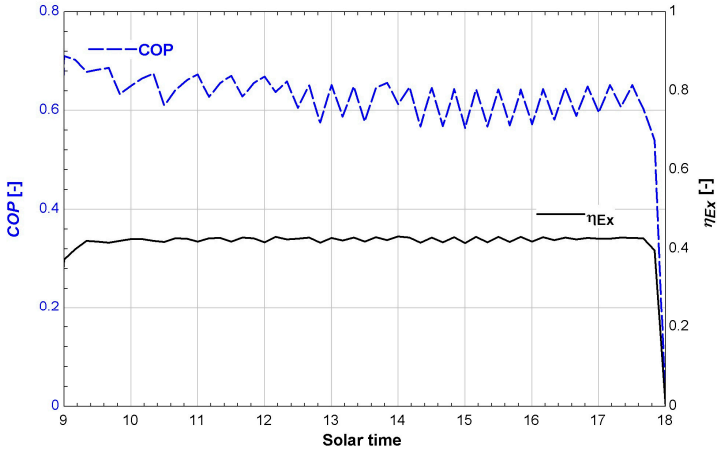

(**b**)

Figure 15. Achieved versus optimum main ST water temperature (**a**) and COP and ACS exergetic efficiency (**b**) for PTC1800 and 90 kg main ST + 140 kg secondary ST, respectively.

5.3. Comparison of Studied Cases

In the present paper, two main cases have been studied, namely a one-volume storage tank and modular storage tank. For the numerical simulation, two commercial PTC have been selected, one having a larger aperture area (PT1-IST), and the other one smaller, but were used as two modules connected in series (PTC1800).

An operating time of the ACS was targeted, as well as its performances in terms of *COP* and exergetic efficiency. The comparison of these results is emphasized in Figures 16–18. As one may see, when comparing one-volume ST ("1ST" in figures) with modular ST ("2ST" in figures), all mentioned results are better in the second case. The operating time is longer, as revealed by Figure 16, a constant high value of the ACS exergetic efficiency is recorded in Figure 17, and the same is true for the *COP* in Figure 18.

As a conclusion, the use of a modular storage tank and controlling the water temperature in the main ST enlarge the operation time interval and improve the ACS performances.

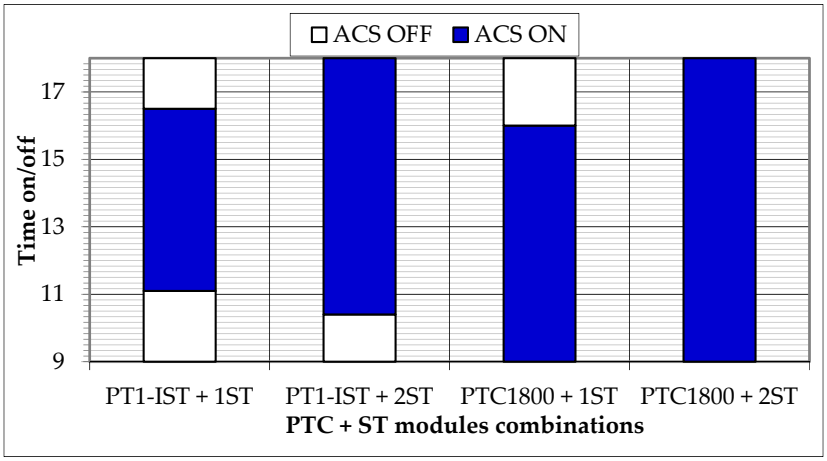

Figure 16. Comparisons of system operating time improvement for modular ST versus one-volume ST, for the two PTC modules, PT1-IST and PTC1800, respectively.

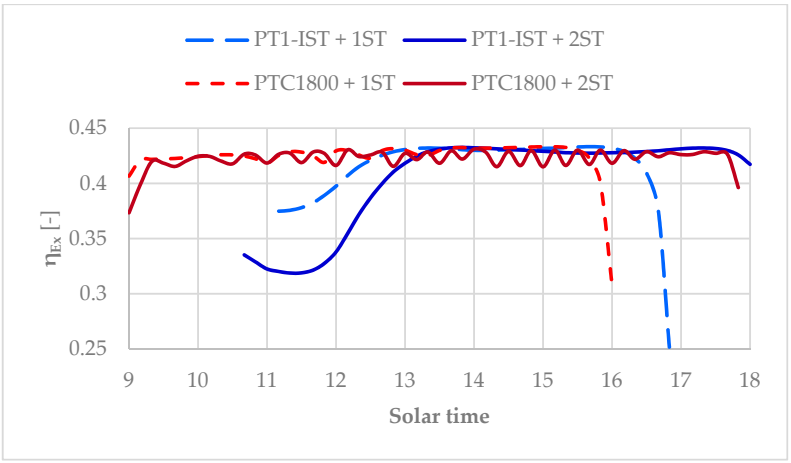

Figure 17. Comparisons of ACS exergetic efficiency improvement for modular ST versus one-volume ST, for the two PTC modules, PT1-IST and PTC1800, respectively.

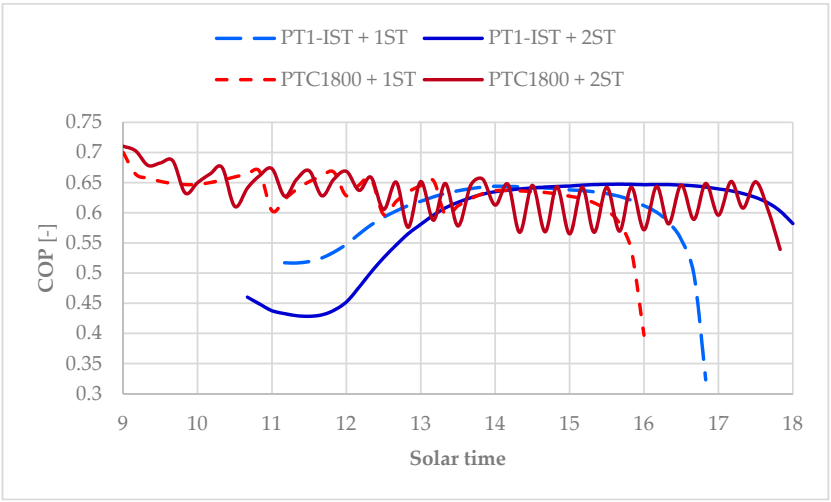

Figure 18. Comparisons of ACS *COP* improvement for modular ST versus one-volume ST, for the two PTC modules, PT1-IST and PTC1800, respectively.

The best choice for the studied case is the use of two commercial PTC1800 collectors connected in series with a modular storage tank with capacities of 90 and 140 kg. The results emphasized that the system operates continuously between 9 am to 6 pm on a calm day (0.2 m/s wind velocity). On a windy day (considering a wind speed of 5 m/s), the computations revealed that the operation time interval is reduced to 9 am to 5:40 pm due to more important PTC losses.

6. Conclusions

In the present paper, a solar absorption cooling system was studied. Its desorber is fed with stored hot water recirculated by a parabolic trough collector. The simulation was done for two commercial PTC, as one may use one larger aperture PTC module or two smaller ones connected in series. Associated storage tank capacities have been determined in both cases, for two system configurations, namely a one-volume storage tank and a modular one, respectively. The numerical results showed that in the case of the one-volume storage tank, the ACS operation time did not cover the entire day for both PTC considered types.

When using a modular storage tank and an operating strategy based on ACS maximum exergetic efficiency, the ACS is maintained in operation for a longer time interval than in the previous case. Also, its performances in terms of *COP* and exergetic efficiency are improved.

Acknowledgments: This work was supported by a grant of the Romanian National Authority for Scientific Research and Innovation, CNCS—UEFISCDI, project number PN-II-RU-TE-2014-4-0846.

Author Contributions: Camelia Stanciu contributed to the development of the model and EES programming; Dorin Stanciu contributed to the design of the study, and to the analysis and interpretation of the results; Elena-Beatrice Tănase and Adina-Teodora Gheorghian contributed to the state of the art analysis and preparation of the manuscript; Cătălina Dobre contributed to the preparation of the manuscript; and Marius Spiroiu contributed to the preparation of the manuscript and final proof. All authors have read and approved the final manuscript.

Conflicts of Interest: The authors declare no conflict of interest. This work was financially supported by a grant of the Romanian National Authority for Scientific Research and Innovation, having no role in the design of the study; in the collection, analyses, or interpretation of data; in the writing of the manuscript, and in the decision to publish the results.

Abbreviations

The following abbreviations are used in this manuscript:

Normal letters

A	area, m^2
a	recirculation factor
c_p	specific heat at constant pressure, $J \cdot kg^{-1} \cdot K^{-1}$
D	diameter, m
Ex	exergy rate, W
f	circulation ratio
G	solar irradiation, $W \cdot m^{-2}$
H	width, m
h	specific enthalpy, $J \cdot kg^{-1}$
h	convection heat transfer coefficient, $W \cdot m^{-2} \cdot K^{-1}$
L	length, m
$\dot{m}$	mass flow rate, $kg \cdot s^{-1}$
$\dot{Q}$	heat rate, W
T	temperature, K
U	overall heat transfer coefficient, $W \cdot m^{-2} \cdot K^{-1}$
w	velocity, $m \cdot s^{-1}$
$\dot{W}$	power, W

Greek letters

α	absorptivity
ε	emissivity
η	efficiency
τ	time, s
τ	transmittance
λ	thermal conductivity, $W \cdot m^{-1} \cdot K^{-1}$
ξ	LiBr concentration in H_2O-LiBr solution. $kg \cdot kg^{-1}$
σ	Stefann-Boltzman constant, 5.67×10^{-9} $W \cdot m^{-2} \cdot K^{-4}$

Subscripts

a	ambient
Ab	absorber/absorbed
Bt	beam (radiation) on tilt surface
C	condenser
f	fluid inside the receiver
fi	inlet fluid to receiver
fo	outlet fluid from receiver
G	ACS desorber (vapor generator)
Gmed	mean value, referring to generator
gls,i	interior glass cover surface
gls,e	exterior glass cover surface
i	inlet
loss	losses
o	outlet
opt	optical
P	pump
pe	exterior pipe wall
pe	interior pipe wall
PTC	parabolic trough collector
rec	recirculated
ST	(main) storage tank
ST2	secondary storage tank
u	useful
v	vaporization
0	refrigerant

References

1. Perez-Lombard, L.; Ortiz, J.; Pout, C. A review on buildings energy consumption information. *Energy Build.* **2008**, *40*, 394–398. [CrossRef]
2. Sun, C.; Giles, H.; Xu, G.; Lan, L.; Lian, Z. Investigation on thermal comfort and energy conservation of local ventilation. *HVAC&R Res.* **2013**, *19*, 584–592. [CrossRef]
3. Marletta, L. Air Conditioning Systems from a 2nd Law Perspective. *Entropy* **2010**, *12*, 859–877. [CrossRef]
4. Li, Z.F.; Sumathy, K. Technology development in the solar absorption air-conditioning systems. *Renew. Sustain. Energy Rev.* **2000**, *4*, 267–293. [CrossRef]
5. Li, M.; Xu, C.; Hassanien, R.H.E.; Xu, Y.; Zhuang, B. Experimental investigation on the performance of a solar powered lithium bromide-water absorption cooling system. *Int. J. Refrig.* **2016**, *71*, 46–59. [CrossRef]
6. Mazloumi, M.; Naghashzadegan, M.; Javaherdeh, K. Simulation of solar lithium bromide–water absorption cooling system with parabolic trough collector. *Energy Convers. Manag.* **2008**, *49*, 2820–2832. [CrossRef]
7. Lu, Z.S.; Wang, R.Z. Experimental performance investigation of small solar air-conditioning systems with different kinds of collectors and chillers. *Sol. Energy* **2014**, *110*, 7–14. [CrossRef]
8. Bellos, E.; Tzivanidis, C.; Antonopoulos, K.A. A detailed working fluid investigation for solar parabolic trough collectors. *Appl. Therm. Eng.* **2017**, *114*, 374–386. [CrossRef]

9. Tzivanidis, C.; Bellos, E. The use of parabolic trough collectors for solar cooling—A case study for Athens climate. *Case Stud. Therm. Eng.* **2016**, *8*, 403–413. [CrossRef]
10. Stanciu, C.; Stanciu, D.; Gheorghian, A. Thermal analysis of a solar powered absorption cooling system with fully mixed thermal storage at startup. *Energies* **2017**, *10*, 72. [CrossRef]
11. Soriga, I.; Gheorghian, A.T.; Stanciu, C.; Stanciu, D. Instability in operation of a solar powered H2O-LiBr absorption cooling system. In Proceedings of the 6th International Conference on Thermal Equipment, Renewable Energy and Rural Development TE-RE-RD 2017, Moieciu de Sus, Romania, 8–10 June 2017; Negreanu, G., Dutu, C., Eds.; Politehnica Press: Bucarest, Romania, 2017; pp. 155–160.
12. Porumb, R.; Porumb, B.; Balan, M. Numerical investigation on solar absorption chiller with LiBr-H_2O operating conditions and performances. *Energy Procedia* **2017**, *112*, 108–117. [CrossRef]
13. Stanciu, C.; Stanciu, D.; Tănase, B.; Gheorghian, A.; Dobre, C. Storage Tank Mass Control for Optimum Solar-Powered Absorption Cooling System Operation. In Proceedings of the 8th International Conference on Energy and Environment (CIEM 2017), Bucharest, Romania, 19–20 October 2017.
14. Stanciu, D.; Stanciu, C.; Paraschiv, I. Mathematical links between optimum solar collector tilts in isotropic sky for intercepting maximum solar irradiance. *J. Atmos. Sol.-Terr. Phys.* **2016**, *137*, 58–65. [CrossRef]
15. *Meteonorm Software*, Version 7.1.8.29631; Global Meteorological Database for Engineers, Planners and Education; Meteotest Genossenschaft: Bern, Switzerland, 2016.
16. Stanciu, C.; Stanciu, D.; Dobrovicescu, A.; Feidt, M.; Gheorghian, A.; Costea, M. Comparative analysis of two arrangements of one stage absorption refrigeration systems. In Proceedings of the Colloque Franco-Roumain Energy, Environment, Economie et Thermodynamique—COFRET'14, Paris, France, 23–25 April 2014; pp. 217–224.
17. Gheorghian, A.T.; Stanciu, C.; Stanciu, D.; Ioniţă, C.; Tănase, B. Versatility study of NH_3-H_2O and H_2O-LiBr absorption refrigeration systems to different operating conditions. In Proceedings of the Thermodynamics National Conference with International Participation SRT'17 (NACOT 2017), Craiova, Romania, 25–27 May 2017.
18. *Engineering Equation Solver*; Academic Commercial Version V9.915; F-Chart Software: Madison, WI, USA, 2015.
19. Grigoriu, M. *Design and Computation of Refrigerating Systems*; University Politehnica of Bucharest: Bucharest, Romania, 1985. (In Romanian)
20. Vasilescu, E.E. *Absorption and Ejection Refrigerating Systems—Theory and Applications*; Printech Publishing House: Bucharest, Romania, 2003. (In Romanian)
21. Radcenco, V.; Grigoriu, M.; Duicu, T.; Dobrovicescu, A. *Refrigerating and Cryogenic Systems—Applications for Engineers*; Editura Tehnica Publishing House: Bucharest, Romania, 1987. (In Romanian)
22. Osta-Omar, S.; Micallef, C. Mathematical Model of a Lithium-Bromide/Water Absorption Refrigeration System Equipped with an Adiabatic Absorber. *Computation* **2016**, *4*, 44. [CrossRef]
23. Osta-Omar, S.; Micallef, C. Determination of Concentration of the Aqueous Lithium–Bromide Solution in a Vapour Absorption Refrigeration System by Measurement of Electrical Conductivity and Temperature. *Data* **2017**, *2*, 6. [CrossRef]
24. Fernandez-Garcia, A.; Zarza, E.; Valenzuela, L.; Perez, M. Parabolic-trough solar collectors and their applications. *Renew. Sustain. Energy Rev.* **2010**, *14*, 1695–1721. [CrossRef]
25. Soliterm GmbH Company (Turkey, Germany). Available online: http://www.solitem.de/ (accessed on 1 October 2017).
26. Kalogirou, S.A. A detailed thermal model of a parabolic through collector receiver. *Energy* **2012**, *48*, 298–306. [CrossRef]
27. Dudley, V.E.; Colb, G.J.; Sloan, M.; Kearney, D. *Test Results: SEGS LS-s Solar Collector*; SAND94-1884 Report; The Smithsonian/NASA Astrophysics Data System: Albuquerque, NM, USA, 1994.
28. McAdams, W.H. *Heat Transmission*, 3rd ed.; McGraw Hill: New York, NY, USA, 1954.
29. Duffie, J.; Beckman, W. *Solar Engineering of Thermal Processes*; John Wiley & Sons Inc.: Hoboken, NJ, USA, 2006.